Homogeneous Linewidth and Relaxation Time Measurements on Rare-Earth-Ion-Doped Crystals

Rauhut, Nina; Ohser, Sabine

2004

Homogeneous linewidth and relaxation time measurements on rare–earth–ion–doped crystals

Sabine Ohser Nina Rauhut

Lund Institute of Technology, May 2004

Abstract

In this report homogeneous linewidth and relaxation time measurements on rare-earth-ion-doped crystals are presented. The experiments have been done in order to assess the suitability of Pr^{3+}:$KY(WO_4)_2$ and Ho^{3+}:$LuVO_4$ as hardware materials for quantum gates.

By conducting a two pulse photon echo experiment on the $^3H_4$–$^1D_2$ transition of Pr^{3+}:$KY(WO_4)_2$, the coherence time was determined to be 13 μs. A lifetime of 44 μs for the excited state was obtained from the decay of the fluorescence light. For the $^5I_8$–$^5F_5$ transition of Ho^{3+}:$LuVO_4$ a coherence time of 16 ns was measured by spectral hole burning. Materials with longer coherence times exist and are therefore more suitable for the implementation of quantum gates than these two crystals.

Contents

1 Introduction

This report is the product of 15 ECTS of project work. It was done in the Photon Echo Group, part of the Atomic Physics Division at Lund Institute of Technology, Sweden.
The project in the field of quantum information processing is connected to a collaboration work between reasearch groups in Orsay, Paris, Caen, Aarhus, and Lund. It concerns **E**xperimental realisation of quantum gates and development of **S**calable **QU**antum computer schemes **I**n **R**are–**E**arth–ion–doped inorganic crystals (ESQUIRE).
This section aims to give a brief introduction to quantum computing in order to explain the connection between our work and the ESQUIRE project.
In a classical digital computer, all information is represented using bits. A bit (short for binary digit) is either 0 or 1, but cannot be both at the same time. A qubit (short for quantum binary digit) can be 0, 1, or a superposition of 0 and 1. Therefore, a single qubit contains much more information than a regular bit. Instead of just holding 0 or 1, a qubit records two complex numbers. Now suppose that we have two regular bits: they can be either in state 00, 01, 10, or 11. A quantum computer operates with a superposition of these states, $a_1|00> + a_2|01> + a_3|10> + a_4|11>$, where a_1, a_2, a_3, and a_4 are complex numbers. This means that two qubits hold 2^2 complex numbers. L qubits hold 2^L complex numbers i.e. the amount of information increases exponentially as the number of qubits grows. That's why it is possible to run certain algorithms much faster on a quantum computer than on a classical computer.
One physical system representing a qubit is a two level atom. The atom can be either in the ground state, in the excited state or in a superposition of both states. In order to perform elementary quantum operations, quantum logic gates are needed. A quantum logic gate is the counterpart of a classical logic gate, except that it can create and perform operations on quantum superpositions. The atom has to remain in a superposition of states while the operation is performed: therefore a large coherence time, T_2, is required.
There have been several suggestions for how to implement quantum gates. A very promising possibility are rare–earth–ion–doped crystals, because they have a large coherence time due to a narrow homogeneous broadening. Furthermore, they fulfill another requirement, namely the possibility to make each qubit interact with the other qubits. When an ion gets excited, its permanent dipole moment changes. This change shifts the absorption frequency

of other nearby ions and thus enables ions to interact.
The aim of our experiments was to assess the suitability of crystals collected by the French co–operators as test materials for quantum gates. The assessment was done on Pr^{3+}:$KY(WO_4)_2$ and Ho^{3+}:$LuVO_4$.

2 Theory

2.1 Rare-Earth-Ion-Doped Crystals

2.1.1 Homogeneous Linebroadening

Rare–earth elements are those elements with atomic numbers between 57 (Lanthanum) and 70 (Ytterbium). The special electron configuration of these elements makes them interesting candidates for the ESQUIRE project.
The $5s$, $5p$ and $6s$ shells are full while the $4f$ shell is only partially filled. In Lanthanum, the number of electrons in the $4f$ shell is zero and increases to 14 for Ytterbium that has a closed $4f$–shell. The $4f$ electrons are shielded by the electrons of the outer orbitals and thus interact only weakly with the environment: therefore, transitions involving $4f$ electrons can have a very narrow linewidth, i.e. the homogeneous broadening is very small (1 to 10 kHz).

2.1.2 Inhomogeneous Linebroadening

When rare–earths are doped into a crystal, the $4f-4f$ transition frequencies aquire a shift. The shielding of the $4f$–orbitals is not perfect and therefore interactions occur with the electric field of the crystal. Because of chemical impurities, lattice imperfections, and strains within the crystal, different ions have slightly different surroundings, resulting in an inhomogeneously broadened absorption profile. This broadening is in the range of hundreds of MHz to hundreds of GHz. The homogeneous and the inhomogeneous linebroadening is shown in figure 1.

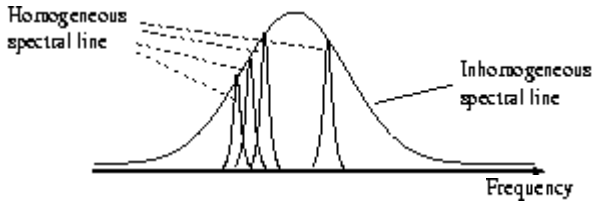

Figure 1: Inhomogeneous and homogeneous linebroadening

2.2 Coherence Time T_2

In order to simplify the theoretical description, we assume an atom with only two energy levels. After a measurement, the atom is found either to be in state 1 or in state 2, but if no measurement is done, it can exist in a coherent superposition of these two states. There is an infinite number of possible superpositions that can be described by

$$|\Psi>= c_1(t)|1> +c_2(t)e^{-iw_{12}t}|2> \tag{1}$$

where $|1>$ and $|2>$ are the wavefunctions of state 1, and state 2 respectively, c_1 and c_2 are the complex amplitudes and w_{12} is the transition frequency. The probabilities to find the atom in state 1, and in state 2 respectively are $|c_1(t)|^2$ and $|c_2(t)|^2$. An atom is said to be in an equal superposition if $|c_1(t)| = |c_2(t)|$. The probability to find the atom either in state 1 or in state 2 is 1, i.e.

$$|c_1(t)|^2 + |c_2(t)|^2 = 1 \tag{2}$$

An atom in a superpositon of two states emits light of a frequency equal to the transition frequency w_{12} between the two states.
The time during which an atom in a superposition of two states can radiate at its eigenfrequency without any perturbation is called coherence time and is denoted by T_2. Other names for T_2 are the homogeneous dephasing time or phase memory time. An atom cannot prevail forever in a coherent superposition of states, i.e. $T_2 < \infty$. This is due to the fact that the lifetimes of the two states are finite. T_2 is usually much shorter than these lifetimes.
T_2 is related to the homogeneous linewidth Γ_h by

$$\Gamma_h = \frac{1}{T_2\pi} \tag{3}$$

There are several phenomena that contribute to the decrease of T_2, and the increase of Γ_h respectively. In solids, like the rare–earth–ion–doped crystals, they are:

1. **Phonon interactions**
   The atoms loose their phase memory due to interactions with the vibrating atoms in the host crystal. This effect can be reduced by cooling the crystal and becomes negligible below 4 K.

2. **Magnetic interactions**
   These are spin–spin interactions between the host atoms and the dopant atoms. Nuclear spin–flips in the host atoms can occur due to the energy degeneracy of oppositely directed spins. They generate a magnetic field which induces spin–flips in the neighbouring dopant atoms. This effect can be reduced by applying an external magnetic field, which breaks the energy degeneracy. If the magnetic field is strong enough, all spins are maintained in one direction, because the energy difference between spin–up and spin–down is too large to be overcome.

The homogeneous linewidth Γ_h can be written as a sum of all individual contributions:

$$\Gamma_h = \Gamma_{Natural} + \Gamma_{Phonon} + \Gamma_{Magnetic} \tag{4}$$

where $\Gamma_{Natural}$ is the natural linewidth due to the Heisenberg uncertainety principle or, equally, the lifetime of the excited state. Γ_{Phonon} and $\Gamma_{Magnetic}$ are the contributions of the described phenomena.
Furthermore, T_2 depends on the density of excited states. If an atom is excited, a change of its electric dipole moment occurs. This change can shift the transition frequency of neighbouring atoms and therefore T_2 decreases. The density of excited states depends on the dopant level and the excitation–pulse energy.

2.3 Bloch Vector Model

A convenient way to illustrate the state of a two level atom is the Bloch vector model. Three variables w, u, v are introduced:
The population of the two levels is expressed by w:

$$w(t) = |c_2(t)|^2 - |c_1(t)|^2 \tag{5}$$

For the ground state, $c_1(t)$ is 1 and $c_2(t)$ is 0, and thus w is -1. For an equal superposition w is 0, while for the excited state w is $+1$.
An atom in a superposition state behaves like a dipole oscillating at the transition frequency. The variables u and v are used to characterize the emitted radiation. They are proportional to the polarisation of the dipoles. u describes the polarisation that is in phase and v describes the polarisation that is 90° out of phase with the electric field of the incoming light. Light emitted from a dipole is always 90° out of phase with its polarisation. Therefore, v

describes the emitted light that is 180° or 0° (depending on the sign of v) and u the light that is 90° out of phase with the incoming light.
A state of an atom described by the three variables w, u and v can be illustrated by a three–dimensional vector in the Bloch sphere.

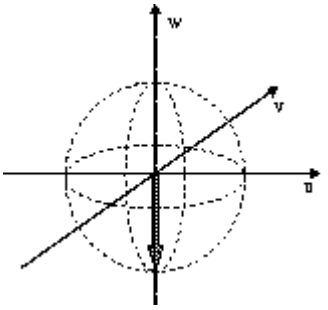

Figure 2: Illustration of the ground state in the Bloch sphere

The ground state of an atom, for example, corresponds to a vector pointing from the origin of the sphere along the w–axis (figure 2). u and v are zero because an atom in the ground state does not radiate.

2.4 Two Pulse Photon Echo

If, under the right conditions, two light pulses resonant with an atomic transition are sent into an absorbing sample, e.g. a rare–earth–ion–doped crystal, a signal called a photon echo can be observed. It is emitted after a time that is equal to the time separation of the two pulses (figure 3).

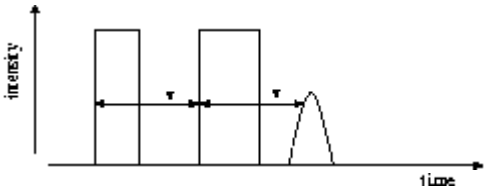

Figure 3: The two pulse photon echo

In order to analyse this effect the Bloch vector model is used. First we assume that all atoms are in the ground state. Therefore the resulting Bloch

vector points along the w–axis (see figure 4(a)). Sending in a laser pulse, that is tuned to the transition frequency, the atoms start to interact with the incoming light. If the pulse is suitable in intensity and duration, it can move the Bloch vector, so that it points along the v–axis (figure 4(b)). Such a pulse is called $\frac{\pi}{2}$–pulse, because it rotates the Bloch vector by an angle of 90° and it transfers the atom into an equal superposition of its two states.
The u–component is zero right after this pulse because all atoms start to radiate at the same time and are all 180° out of phase with the incoming radiation. The induced macroscopic dipole moment decays rapidly since the atoms come out of phase because of their slightly different eigenfrequencies. This decay is called free induction decay. The dephasing process is illustrated in the Bloch sphere by the vectors spreading out in the uv–plane (figure 4(c)).
A second pulse is sent in after a time τ. The time separation of the two pulses has to be short compared to the lifetime of the upper state in order to assure that no atoms decay to the ground state before the second pulse is sent in. The second pulse is a π–pulse, i. e. two $\frac{\pi}{2}$–pulses with zero separation. The radiation of the atoms and the incoming light will interfere.
The v– component is 180° out of phase and therefore interferes destructively with the electric field of the incoming radiation. Destructive interference causes a decrease in the total intensity and can therefore be interpreted as absorption. The atoms become excited by absorbing a photon. The first part of the π–pulse turns the Bloch vector by 90°, so that it points along the w–axis. Since all atoms are in the excited state, the only possible interaction results in de–excitation. The second part of the π–pulse therefore transferes the atoms back to an equal superposition of states and causes the Bloch vectors to return to the uv–plane (figure 4(d)). The result is a change in sign of v.
There is a phase factor of 90° between the u–component and the electric field of the incoming radiation. This phase factor does not cause any interference effect and the resulting intensity is just the sum of the two single intensities. Therefore, the u–components of the Bloch vectors do not change.
Leaving the atoms evolving freely, a rephasing of the radiation occurs and the individual Bloch vectors become aligned along the v–axis (figure 4(e)). This happens at the time 2τ, because the rephasing process takes as much time as the dephasing process. The result is a macroscopic dipole moment and a photon echo can be observed.

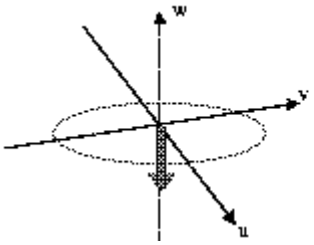

(a) All the atoms are in the ground state

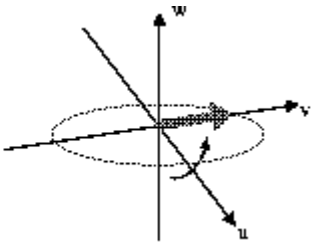

(b) After a $\frac{\pi}{2}$–pulse they are transfered to an equal superposition of states

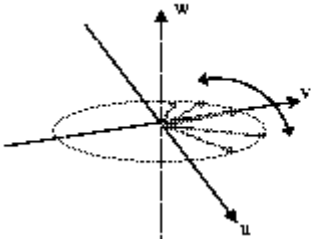

(c) The individual atoms come out of phase

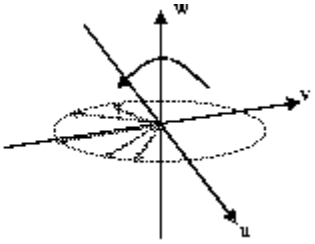

(d) A π–pulse changes the sign of the v–component

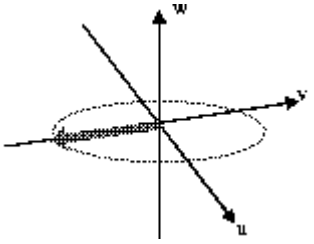

(e) After a time that is equal to the time separation between the two pulses all atoms are in phase again. A photon echo is emitted.

Figure 4: Pictorial visualisation of the generation of the two pulse photon echo using the Bloch vector model

2.5 Determination of T_2 by Using Photon Echoes

Phase perturbing events make the atoms to forget their phases, repress the rephasing process and therefore decrease the photon echo intensity. If the coherence time T_2 is very short, no photon echo can be observed, because the atoms have to remain in a superposition all the time from the first excitation pulse until the emission of the photon echo.
If T_2 is large enough and a photon echo is emitted, the dependence of its intensity on the time between the two excitation pulses makes it possible to determine T_2. By increasing the time between the two excitation pulses the probability that the phases are randomised is enhanced and the intensity of the echo signal is decreased. But how are the echo intensity and T_2 connected?
Every atom is radiating at a certain eigenfrequency. The resulting electric field is the sum of all individual contributions and decays exponentially when the atoms get out of phase. It is related to T_2 by

$$E(t) = E_0 \cdot e^{-\frac{t}{T_2}} \tag{6}$$

The intensity of the photon echo signal I is

$$I(t) = I_0 \cdot e^{-\frac{t}{\tau_{echo}}} \tag{7}$$

where τ_{echo} is the decay time of the echo. The intensity is related to the electric field by

$$I(t) = |E(t)|^2 = E_0^2 \cdot (e^{-\frac{t}{T_2}})^2 = I_0 \cdot e^{-\frac{-2t}{T_2}} \tag{8}$$

According to equation (7) and (8) the coherence time is twice the echo decay time. However, this time is only the time from when the second pulse was sent in until the time when the atoms cease to be in a coherent superposition. In order to observe an echo, the atoms have to remember their phases from the first pulse on. This yields another factor of two and therefore the echo decay time has to be multiplied by four.

$$T_2 = 4\tau_{echo} \tag{9}$$

2.6 Spectral Hole Burning

Dopant ions in a crystal experience an electric field that is determined by the characteristics of the host material. Because of quadrupol interactions, degenerated states of the ions can be split into hyperfine levels. The energy difference between the levels is in the range of a few MHz to GHz.
Let us consider an atom with two states that are both split into hyperfine levels. When a transition is induced from one level in the ground state to another level in the excited state, the atom will first stay in this excited state and later relax to one of the ground state levels. A continuous excitation, achieved by sending in a long pulse at a fixed transition frequency ν, can cause a level depletion in the ground state. The new configuration, that is generated by this burn pulse, results in a high transmission of light at the frequency ν.
A second pulse is sent in after a time σ. This long read–out pulse is weak, so that it disturbs the system only marginally. It is tuned over a wide frequency range which includes the frequency ν. In the absorption profile a hole appears at this frequency where the crystal is now transparent (see figure 5). The absorption from this empty level to the other levels in the excited state will also be smaller and show up as side–holes at the corresponding frequencies. In addition some anti–holes turn up due to the increased absorption because levels in the ground state have increased population. The hyperfine level splitting can be determined from the distances between all these modifications of the smooth absorption profile.

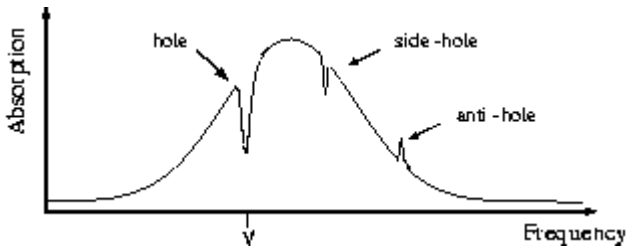

Figure 5: The absorption profile as probed after a hole burning experiment

The lifetime of the hole is determined by two contributions: The relaxation between the excited state and the depleted ground state level on the one side, and on the other side, the relaxation between different hyperfine levels.

Therefore, the depth of the hole as a function of the time between the burn and the read–out pulse is a combination of two exponential decays.
As described in section 2.2, T_2 and the homogeneous linebroadening are related by

$$T_2 = \frac{1}{\pi \, \Gamma_h}$$

Measuring the hole's FWHM gives the value for Γ_h. It is an additional method for determining the coherence time and is used if T_2 is too short for photon echo experiments.

2.7 Lifetime T_1

The term T_1 denotes the lifetime of the excited state.
The excited atoms relax to the ground state by emitting radiation. If the ground state is splitted into hyperfine levels, transitions to different ground state levels are possible. Therefore, the emitted radiation can be frequency shifted compared to the absorbed radiation. The emitted radiation is called fluorescence light and its intensity decays exponentially by

$$I(t) = I_0 \cdot e^{-\frac{t}{T_1}} \tag{10}$$

where T_1 is the decay constant that is equal to the lifetime of the excited state.

3 Equipment

3.1 Samples

Experiments were performed on two different crystals. One was doped with Praseodymium (0.1%) and the other was doped with Holmium (0.1%): Pr^{3+}:$KY(WO_4)_2$ and Ho^{3+} : $LuVO_4$.
The electronic configuration of Pr^{3+}–ions is $4f^2$ which gives rise to a ground state of $^3H_4$. We induced the transition to the excited state $^1D_2$. The energy difference between these two levels corresponds to a wavelength of 612.97 nm [11]. Both the ground and the excited state are split into three hyperfine levels.
The electronic configuration of $4f^{10}$ of the Ho^{3+}–ions results in the ground state $^5I_8$ and the transition of interest is the one to the $^5F_5$ level. Since the separation between these energy levels is smaller than in the Praseodymium doped crystal, a higher wavelength (649.005 nm) was required.

3.2 Laser System

A *Coherent* CR–699–21 ring dye laser pumped by a *Spectra Physics* Ar^+–ion laser was used for the experiments (see figure 6). A ring dye laser uses dye solution as active medium and its resonator is formed into a ring by means of multiple mirrors. The CR–699–21 is a single frequency, tunable, stabilized, travelling wave ring dye laser.

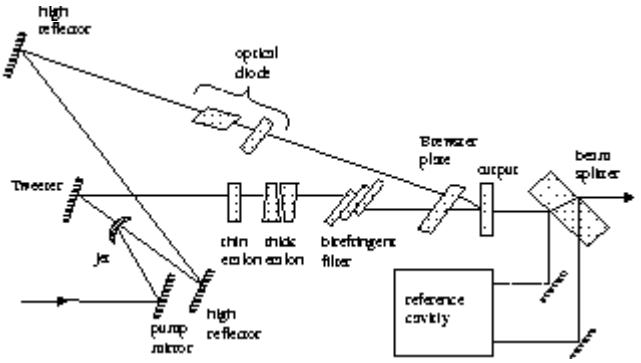

Figure 6: The simplified optical schematics of the CR–699–21 laser

For running the experiments with the Pr^{3+}–doped crystal we used Rhodamine 6G dye and for the Ho^{3+}–doped crystal the dye was exchanged for Rhodamine 101. The output power of the dye laser was in the range of 80 to 200 mW during all the measurements.
The main feature of a ring dye laser is an undirectional, travelling wave operation i.e. an oscillation in a preferred direction achieved by inserting an optical diode. The laser's single frequency output power can be increased compared to standing–wave linear cavities.
The CR–699–21 operates on single frequency by the use of a three–plate birefringent filter (Lyot filter), a thin etalon, and a piezoelectrically driven thick etalon. The single mode isolation is illustrated in figure 7.
The Lyot filter supresses all oscillation in the dye, except for a band of several hundreds of modes. The number of lasing modes is reduced to approximately ten by a thin etalon, that has a free spectral range of 225 GHz. A thick etalon of 10 GHz free spectral range achieves single–mode operation. The use of these three optical elements results in an effective linewidth of about 30 MHz.

Figure 7: Single mode operation by using a Lyot filter and two etalons ([5])

In order to stabilize the system a portion of the output beam is passed through a reference cavity. It provides a reference signal to the electronics that controls the Brewster plate, the tweeter and the etalons. By this active stabilization process the laser cavity length is adjusted and the oscillating mode is servo–locked to a stable reference point.

3.3 Detectors

3.3.1 Photomultiplier Tube

A photomultiplier tube (PMT) is an extremely sensitive device for detecting optical signals. It consists of a vacuum tube in which a photocathode followed by focussing electrodes, an electron multiplier and an anode is placed. When light strikes the photocathode, photoelectrons are emitted into the vacuum. These photoelectrons are accelerated towards the set of dynodes, where secondary electrons are created. The process of secondary-emission multiplication causes a large increase in the number of electrons. The multiplied electrons are collected by the anode as an output signal.

3.3.2 Photodiode

Photodiodes are not as sensitive as a PMT and have the advantage that they are very small and require little power.
Photodiodes are semiconducting devices that convert light into electrical signals. In principle, a photodiode is a p–n junction that is reverse–biased. That means that a positive bias is applied on the n–side of the diode and a negative bias is applied on the p–side. No current flows in a reverse–biased p–n junction, but as soon as an incident photon strikes the junction, the incident photon is absorbed and an electron-hole pair is created. The electron and the hole are swept through the junction in opposite directions, creating a current in the photodiode.

3.4 Acousto–Optic Modulators

Acousto–optic modulators (AOM) are devices used for the electronic control of laser beams. They consist of optical materials that are used to deflect and modulate the amplitude and to change the frequency of the laser beam.
In our experiments computer controlled electrical pulses are sent to an AOM driver that creates a radiofrequency acoustic wave (RF). The RF enters the AOM and forms a sinusoidal grating within the optical material. When the laser beam passes through the AOM, acousto–optic interaction occurs and the beam is diffracted by this grating into several orders k. In figure 8 the function of an AOM is schematically illustrated. The angular diffraction is linearly proportional to the acoustic frequency ν_a, so that the higher the frequency, the larger the diffracted angle. ν_a can be slightly varied by changing

the tuning voltage , V_T, that controls an internal oscillator of the driver. Furthermore, the laser beam frequency ν_o^k of the diffracted beam k is shifted by an amount equal to the acoustic frequency ν_a as

$$\nu_o^k = \nu_o + k\,\nu_a \tag{11}$$

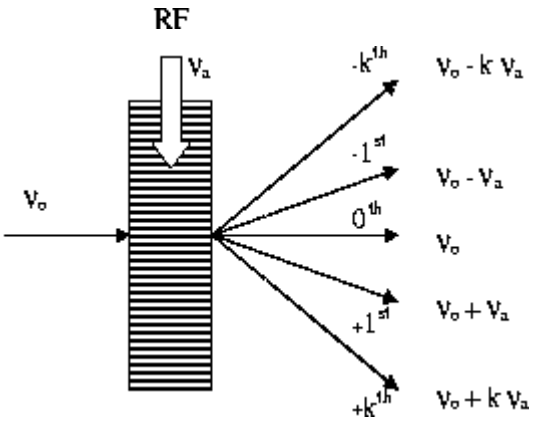

Figure 8: The acoustic–optic modulator

In the experiment three *Isomet 1205C* AOMS were used, controlled by an *Isomet D320* AOM driver. Their optical material is $PbMoO_4$.

3.5 Cryostat

The crystal is placed in a chamber that is filled with liquid helium (4 K) inside a cryostat. To minimise heat transfer, it is set in a high vacuum chamber cooled by liquid nitrogen (77 K). The outer layer of the cooling system is a second high vacuum chamber (see figure 9).
There are three windows in the cryostat. A non negligible amount of energy is lost due to light scattering and reflection by these windows and the liquid helium that surrounds the sample.

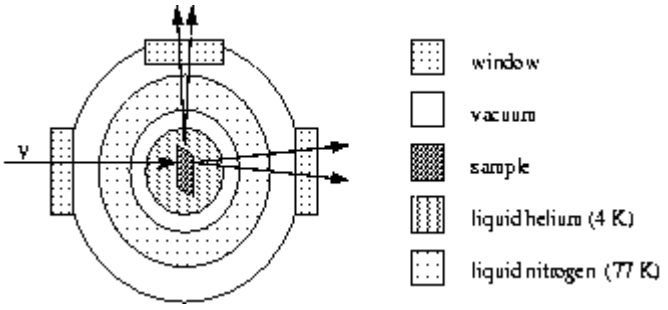

Figure 9: The Cryostat

3.6 Wavemeter

An external digital wavemeter, built in 1980 by Lars–Åke Nilsson and Hans Hertz , LTH Lund [7]was used to determine the laser wavelength. The wavelength is continuously measured by sending a small portion of the laser beam reflected from a glass plate to the wavemeter while conducting the experiment. The external wavemeter functions according to the Michelson interferometer principle. It measures wavelengths in the range of 4000 to 8000 Å with an accuracy of 0.06 Å.
The incoming beam is split into two parts by a beam splitter. The first part goes directly to the detector. The second part covers a longer distance than the first one, as it is sent to a movable mirror. By moving the mirror, the difference in the optical path, ΔL, changes. Thus fringes that are due to the interference of the two beams are detected. Every fringe means a change of λ in the optical path difference. Therefore, the number of counted fringes N and ΔL are related by

$$\Delta L = N\,\lambda \tag{12}$$

To avoid the need for measuring ΔL and N simultaneously, a reference laser with a known wavelength is used (see figure 10).
Both laser beams follow exactly the same optical path, so that ΔL can be expressed as:

$$\Delta L = N\,\lambda = N_{ref}\,\lambda_{ref}$$

As N and N_{ref} are measured and λ_{ref} is known the laser wavelength is determined as:

$$\lambda = \frac{N_{ref}}{N} \lambda_{ref} \tag{13}$$

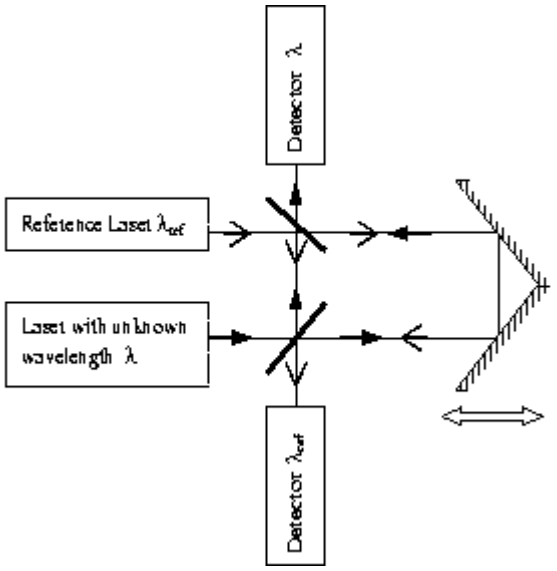

Figure 10: The wavemeter schematics

4 Experiments

All experiments started with mounting the crystal on a holder, putting it into the cryostat, and cooling down the system with liquid nitrogen. After a reasonable time the inner chamber was flooded with helium gas and then it was filled with about 20 cm of liquid helium. The complete cooling process took approximately 24 hours.
In order to keep the temperature low during the measurements, one can (8 liters) of liquid nitrogen was added daily and a level of several centimeters of liquid helium was held in the sample chamber.

4.1 The Two Pulse Photon Echo Experiment

4.1.1 Aim

The aim of this experiment was to determine the coherence time T_2 in Pr^{3+}:$KY(WO_4)_2$ by using the two pulse photon echo.

4.1.2 Set–up

The experimental set–up is shown in figure 11.
The laser beam was divided into two parts by a beam splitter (B1). One part was sent to the wavemeter, while the other part was focussed on an acoustic–optic modulator (AOM) for creating pulses from continuous wave laser radiation. The AOM was adjusted to have the highest possible intensity in the first diffraction order. The zeroth order, which is the unchanged main component, and all higher orders were blocked by an aperture. Since the first order is deflected with respect to the main component, a second AOM was used to compensate this deflection.
The pulses were focussed on the crystal by a 20 cm lens. In order to control the direction and position of the beam to make it pass through the sample, two mirrors (M1 and M2) have been arranged.
The crystal was mounted on a holder which could rotate the sample.

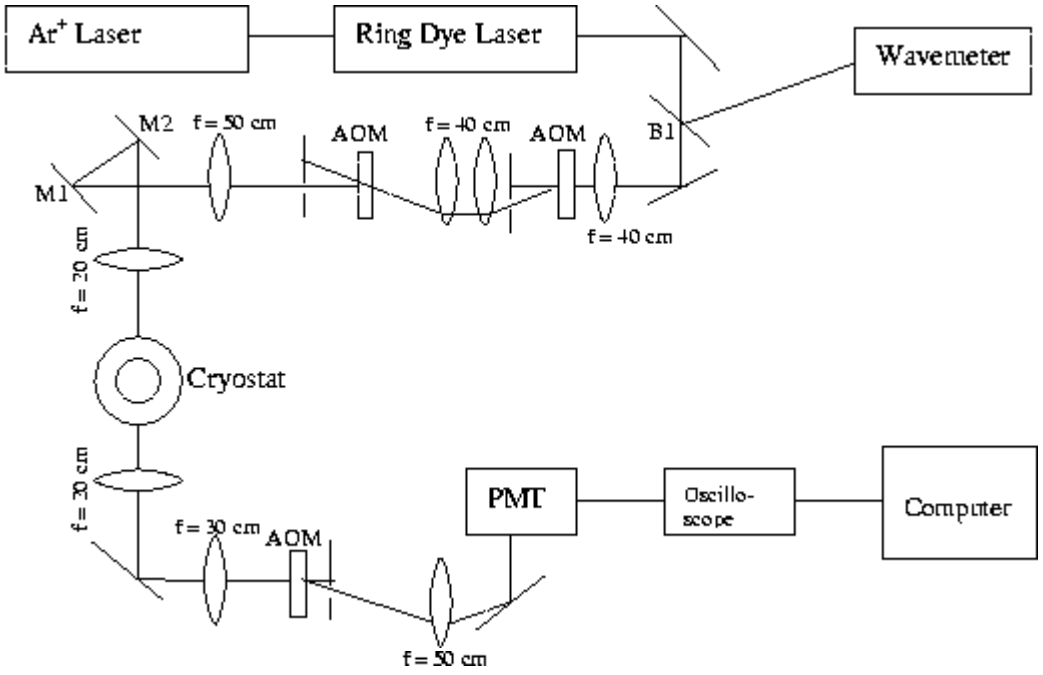

Figure 11: Experimental set–up for the T_2 measurement

Behind the cryostat, a third AOM was set up to block the excitation pulses. This was required because too strong excitation pulses blind the PMT making it impossible to detect a weak echo signal. The blocking was achieved by controlling the AOM with the gate pulse, another electronical pulse generated by the computer. The corresponding time window is defined in such a way that it is open only when the echo signal is transmitted.
Again an aperture suppressed all diffraction components except the first order one. Some scattered light of the main component still reached the PMT. Therefore, the two excitation pulses were still detected, but were attenuated. The output signal of the PMT was recorded by an oscilloscope that was triggered by the pulse T_0. All electronical pulses are illustrated in figure 12.

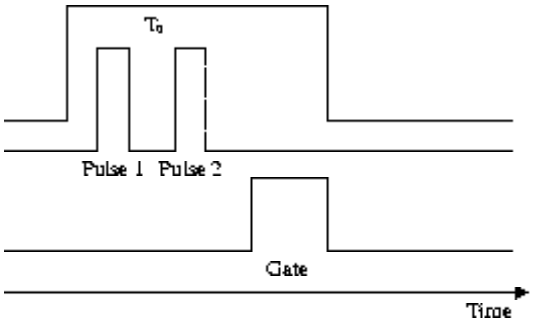

Figure 12: Output signals from the computer

The AOMs were controlled by the RF driver powered by 28 V with a 12 V input to the frequency controlling V_T input. In order to have an continuous beam for the adjustments, the modulation input (MOD) was set to a constant voltage (5 V). The schematics of the AOM electronics is shown in figure 13.

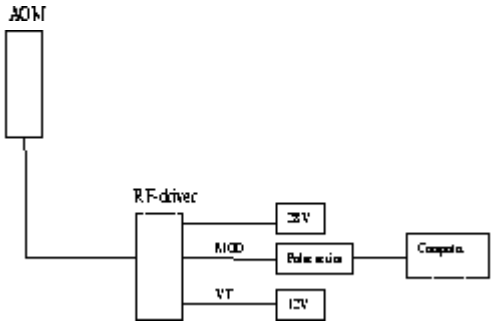

Figure 13: The AOM electronics

4.1.3 Execution

The first step was to tune the laser to the desired transition frequency. The reference value for the transition wavelength was 612.97 nm [11]. We used a photodiode, connected to the oscilloscope, to detect the signal after it passed through the cryostat. When the laser frequency was equal to the transition frequency, the shape of the two excitation pulses changed (see figure 14).

They lost their rectangular shape and the intensity increased slowly with time. This behaviour can be understood in the following way: When a pulse is sent in, most of the atoms are in the ground state and therefore absorb light whose frequency matches a transition frequency. These atoms become excited and the ground state population decreases. As a result, less light can be absorbed: this can be observed as an increase in intensity.

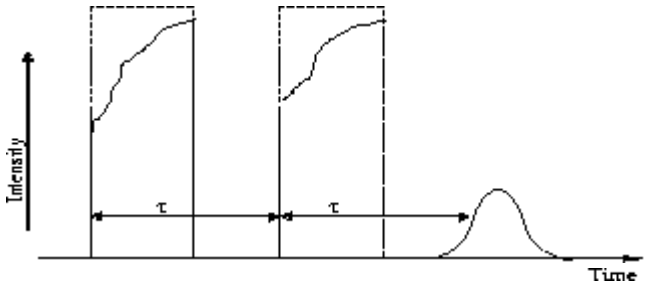

Figure 14: The change of the pulse shape in the case of absorption

We observed absorption at a wavelength of 613.06 nm.
The next step was to detect the photon echo, which we managed to do soon after we had observed absorption. Up to this point, the photodiode was very helpful because it was easy to handle.
In order to make precise measurements, it was necessary to use the photomultiplier. The echo intensity for larger pulse separation becomes too small to be detected by a photodiode.
Before starting the measurements, we optimized the ratio between the echo intensity and the intensity of the scattered light. This was achieved by varying the pulse sequence, changing the polarisation of the laser light by rotating a $\frac{\lambda}{2}$–plate and adjusting the aperture and the two mirrors in front of the photomultiplier.

A very good signal was obtained for this set of values:

duration of the 1^{st} pulse:	500 ns
time between the two pulses:	1500 ns
duration of the 2^{nd} pulse:	500 ns

Another set of measurements was done using the following pulse sequence:

duration of the 1^{st} pulse:	1000 ns
time between the two pulses:	3000 ns
duration of the 2^{nd} pulse:	1000 ns

The measurements were performed by the same computer that we used to generate the electronical pulses sent to the AOM. The program increased the time between the two pulses stepwise, every time integrating the signal accumulated during the time the gate was open. The result is the area under the echo signal – which is proportional to the echo intensity – as a function of the time separation between the two pulses.
The computer plotted these data and the observed curve showed the exponential behaviour that was predicted by equation (7). Furthermore, it calculated the decay constant of the curve, which is equal to the echo decay time. By multiplying this value by four, the value for T_2 was obtained.
We ran these measurements for different excitation pulse energies, as T_2 depends on the density of excited states (section 2.2, page 8). This was done by inserting different attenuators in the optical path. The power was measured in front of the cryostat with a digital power meter. However, this device only measures the average power. In order to get the excitation pulse energy, this value had to be transformed by using the following equation:

$$E_{exc} = \frac{P}{2R} \tag{14}$$

where E_{exc} is the excitation pulse energy, P is the measured power provided by the power meter and R is the repetition rate of the computer pulses in Hz. The factor of two in the denominator takes into account that a sequence consisted of two pulses of the same duration. While the echo intensity was registered, the value for the repetition rate was 10 Hz. For measuring the power, the repetition rate was set to 200 Hz.

4.1.4 Results

Figure 15 shows the result of a single measurement. The echo intensity is plotted as a function of the time separation of the two pulses. By doing an exponential fit, the computer calculated the value for the echo decay time τ_{echo}.

$$\tau_{echo} = 2.96\ \mu s$$

The measured power was 720 nW and the excitation pulse energy, calculated by equation (14), was 1.8 nJ.

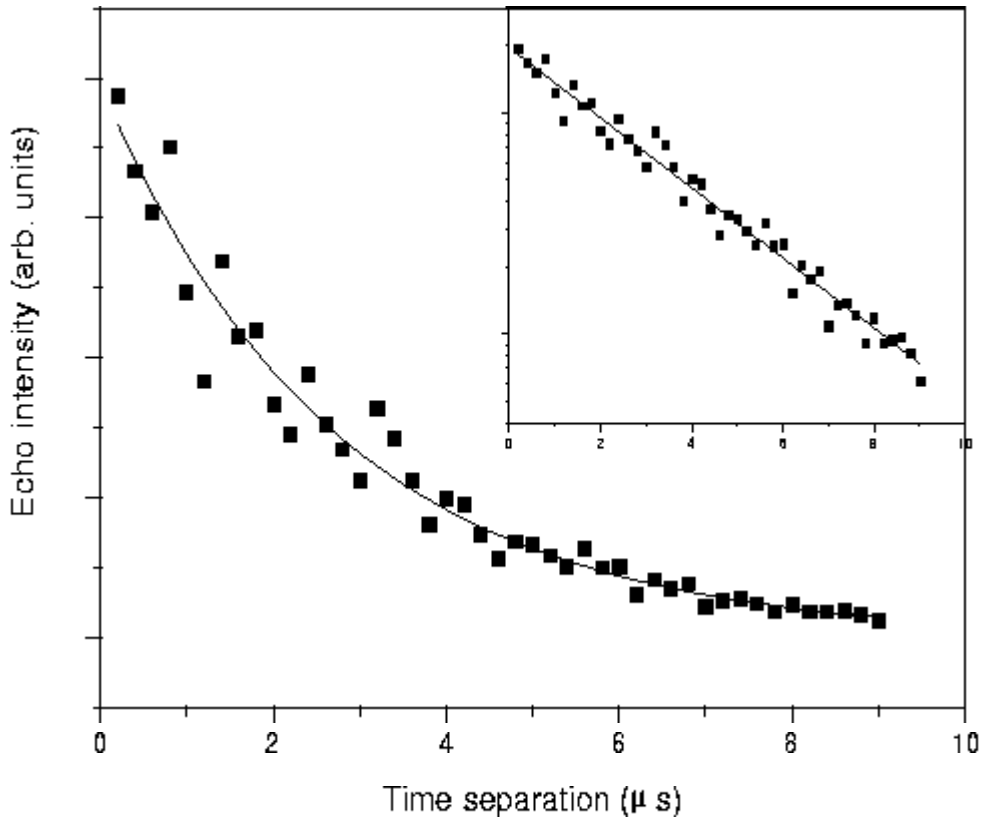

Figure 15: Two photon echo decay plotted on linear and logarithmic scales

In figure 16, the homogeneous linewidth Γ_h is shown as a function of the excitation pulse energy.

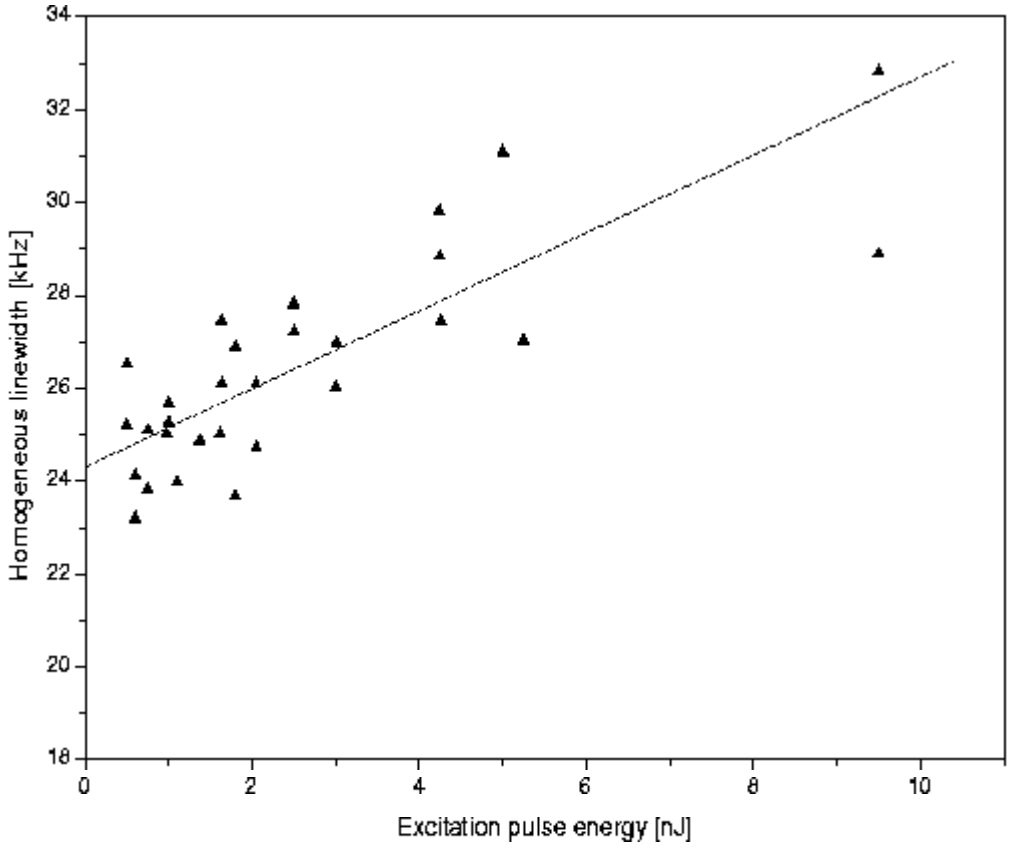

Figure 16: Dependence of the homogeneous linewidth on the excitation pulse energy

The increase of Γ_h, and the decrease of T_2 respectively, with increasing excitation pulse energy as described in the theory can be clearly seen. The excitation pulses constitute a disturbance of the system: therefore, in order to obtain a value for T_2 for zero external disturbance, we did a linear fit extrapolated to zero excitation pulse energy. The values obtained for the homogeneous linewidth Γ_h and the coherence time T_2 are:

$$\Gamma_h = (24.3 \pm 2.9)\, kHz \qquad T_2 = (13.1 \pm 1.6)\, \mu s$$

4.2 Determination of T_1

4.2.1 Aim

The lifetime of the excited state $^1D_2$ of Pr^{3+}:$KY(WO_4)_2$ was measured by determining the decay time of the fluorescence light.

4.2.2 Set–up

The set–up for this experiment is shown in figure 17.

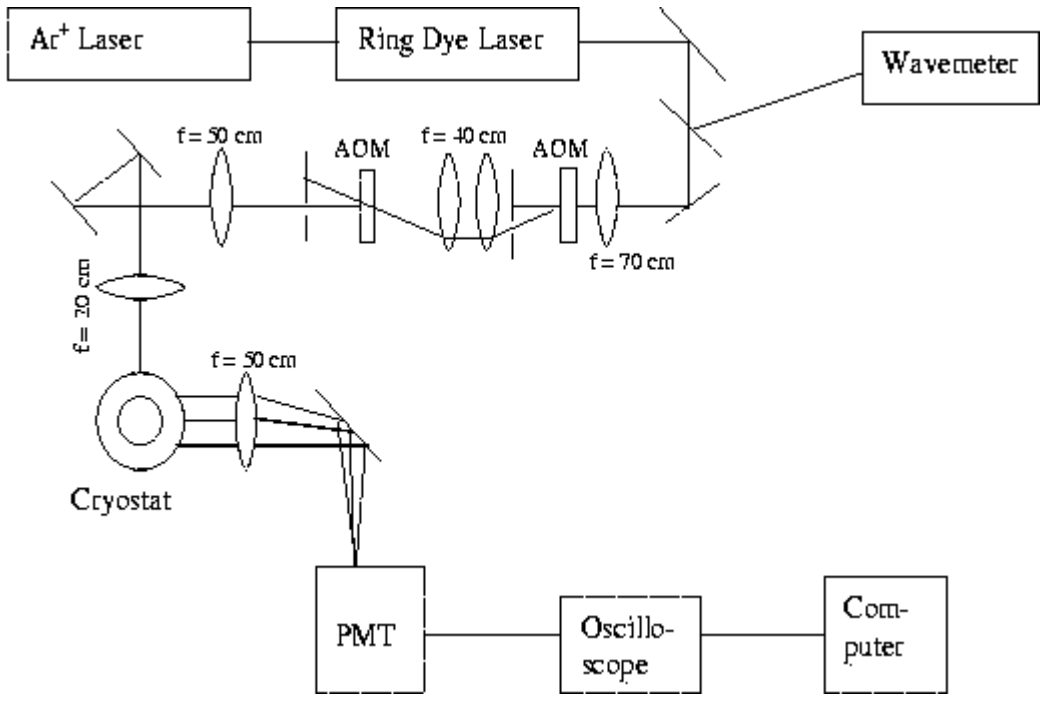

Figure 17: Experimental set–up for the T_1–measurement

The optical path unto the cryostat was not altered. In contrast to the T_2–measurement, the fluorescence light that left the cryostat from the side window was detected.
In order to collect as much of this light as possible, a lens with a large diameter was used to focus the light on the photomultiplier.
A filter in front of the PMT blocked the scattered laser light so that only the frequency–shifted fluorescence light was detected.

4.2.3 Execution

Only one pulse of the transition frequency which is 613.06 nm was sent on the sample.
We observed the output signal of the photomultiplier using an oscilloscope which was connected to the computer. This made it possible to transfer the data of the decay curve from the oscilloscope to the computer for the purpose of analysis.

4.2.4 Results

Figure 18 shows the decay curve of the fluorescence light, and the corresponding exponential fit.
The decay time of this curve, the lifetime of the excited state T_1, is

$$T_1 = (43.8 \pm 2.0)\mu s$$

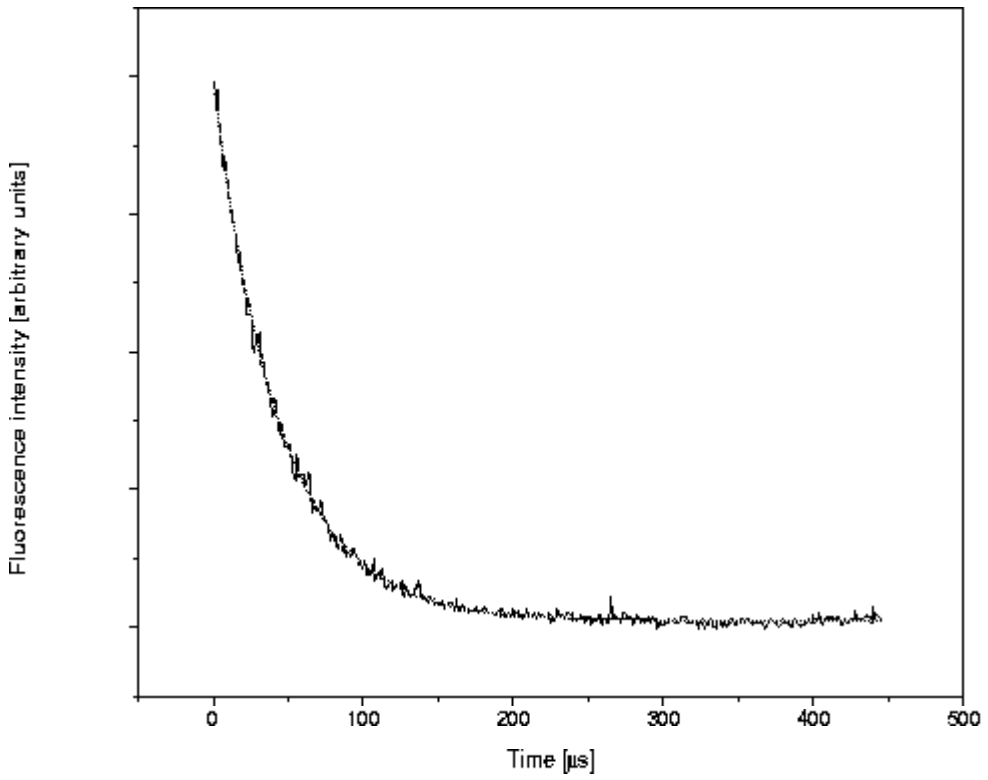

Figure 18: Fluorescence signal of the $^1D_2 - ^3H_4$ transition

4.3 Spectral Hole Burning on Ho^{3+}:$LuVO_4$

4.3.1 Aim

For the crystal Ho^{3+}:$LuVO_4$, we observed absorption at a laser wavelength of 649.19 nm, but no echo was found. Since we could not conduct the two pulse photon echo experiment, we did spectral hole burning in order to obtain a value for T_2.
The lifetime of the hole was also determined.

4.3.2 Set–up

The set–up for this experiment is shown in figure 19.

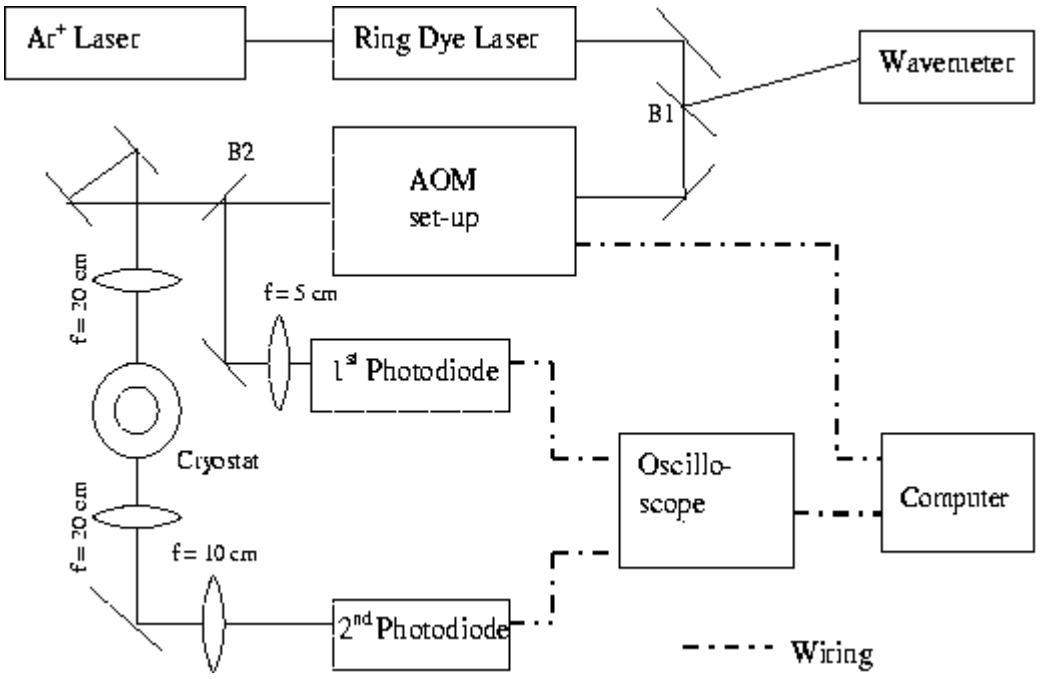

Figure 19: Experimental set–up for hole burning

The two AOM *Isomet* 1205C were exchanged for one AOM *AA Opto–electronic* that has a bandwidth of 100 MHz. Using this device, the laser beam could be electronically controlled as before, but this AOM was capable of larger beam deflections, i.e. the incoming beam could be scanned wider in frequency. This was an advantage because the read–out pulse should be tuned over a large frequency range. The tuning was achieved by applying a ramp pulse, i.e. a pulse whose intensity increases linearly with time, on the V_T input in order to tune the voltage (see figure 21).
In order to keep the optical path straight like in the experimental set–up for the two pulse echo experiment, the light was double–passed through the AOM using a set of mirrors. After passing the AOM set–up, the laser beam was pulsed and shifted in frequency. The detailed AOM set–up can be seen in figure 20.

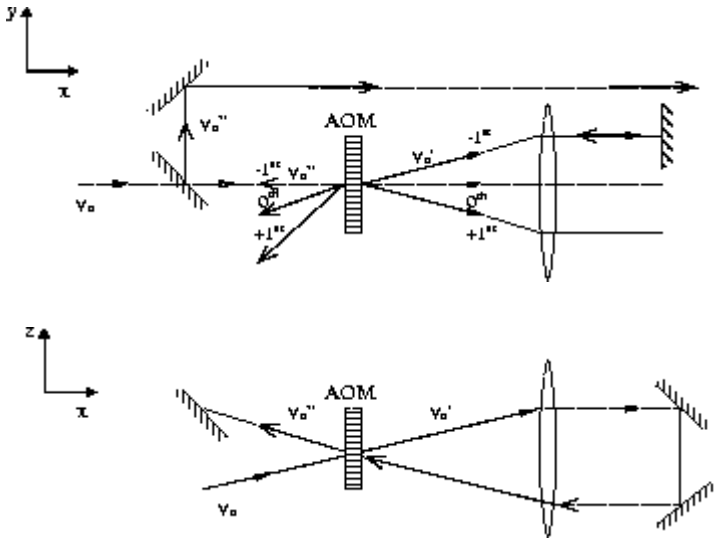

Figure 20: The AOM set–up

In order to do the hole burning measurements, two photodiodes were used. Behind the AOM, the incoming beam was split into two parts by a beam splitter. A small portion was sent to the first photodiode, in order to detect a reference signal. The second portion was sent through the cryostat to another

photodiode that detected the signal. We observed the output signals of the photodiodes using an oscilloscope.

4.3.3 Execution

The process of hole burning consisted of two parts. In the first, a burn pulse caused a level depletion in the ground state of the dopant ions, i.e. the actual hole burning was done. The read–out pulse, that was sent in after a time σ, was used to demonstrate the generated modifications in the absorption profile. This pulse had just half of the intensity of the burn pulse and was tuned over 200 MHz by applying the ramp pulse on the V_T input.
All parameters were controlled by the computer. Three waveforms were defined and put together to form a variable hole burning sequence:

Burn	duration	1 μs
	amplitude	1.0
	frequency	fixed
Wait1mu	time between pulses	1 μs
Readout	duration	30 μs
	amplitude	0.5
	readout width	200 MHz

The depth of the hole decreases with σ. Thus the exponential decay of the hole can be determined by measuring its depth for increasing values of σ. The hole burning sequence was set to

$$200 \cdot \texttt{Burn} + \texttt{k} \cdot \texttt{Wait1mu} + 1 \cdot \texttt{Readout}$$

where $k = 1 \ldots 1800$ is the number of the measurement. The sequence is shown in figure 21.
The signals detected by the photodiodes were sent to an oscilloscope and transfered to the computer using the program LabView. There was a large difference in intensity between the transmission signal detected behind the cryostat and the reference signal detected by the first photodiode. For this reason, the ratio of the two signals, rather than their algebraic difference, was plotted. One example is shown in figure 23.

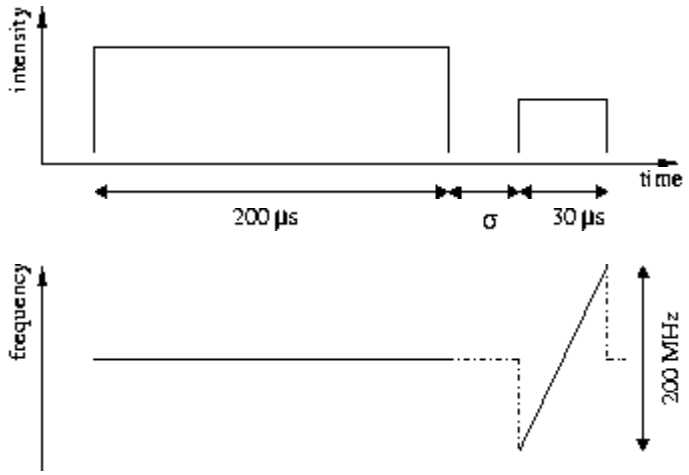

Figure 21: The hole burning sequence

4.3.4 Results

T_2 can be calculated from the hole's linewidth FWHM. Figure 22(a) shows the reference signal, figure 22(b) the read–out signal, and figure 23 the ratio of these two curves for a pulse separation of 150 μs. On this plot a Lorentzian fit was done in order to obtain a value for the homogeneous linewidth.

$$\begin{aligned} \text{FWHM} &= \Gamma_h = 20.3 \text{ MHz} \\ T_2 &= \frac{1}{\pi \, \Gamma_h} = 15.7 \text{ ns} \end{aligned}$$

The linewidth changed slightly with increasing pulse separation σ. The average over all obtained values for T_2 is:

$$T_2 = 15.8 \text{ ns}$$

The standard deviation is 1.7 ns.

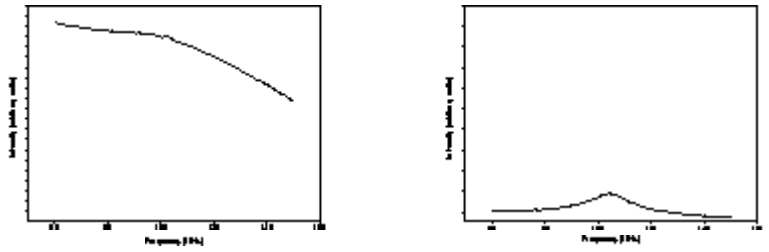

(a) (b)

Figure 22: The reference signal and the read–out signal for a pulse separation of 150 μs

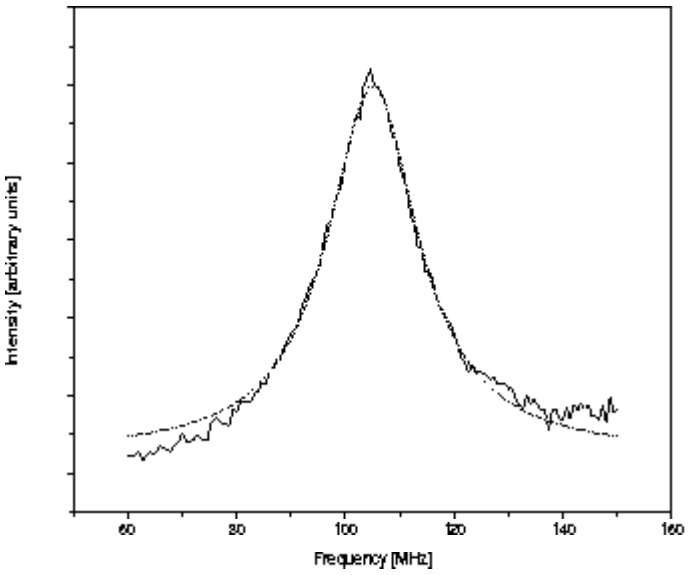

Figure 23: The ratio between the read–out signal and the reference signal

In figure 24, the transmission intensity of the read–out signal is plotted against the pulse separation σ. An exponential fit gives the decay time of the hole that is due to relaxation processes of the excited state to the ground state and relaxation processes between the hyperfine levels of the ground state. From the recorded data it was not possible to distinguish the presence of two different decay processes.

$$\tau = (311 \pm 27)\mu s$$

As no side–holes and no anti–holes could be detected, it was not possible to obtain any information about the hyperfine splitting.

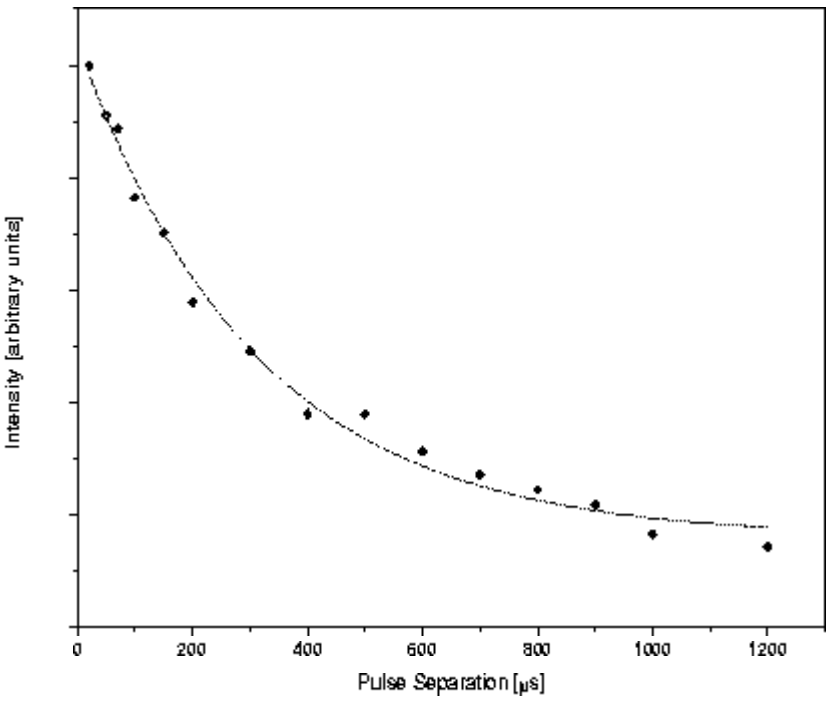

Figure 24: The hole depth as a function of the time σ between the burn and the read–out pulse

5 Conclusion

Using the results of these experiments, it is possible to assess the usefulness of Pr^{3+}:$KY(WO_4)_2$ and Ho^{3+}:$LuVO_4$ for the ESQUIRE project.
In the theory section of this report, we pointed out that the suitability for the implementation of a quantum gate is largely determined by the coherence time, T_2.
The first crystal that we tested, Pr^{3+}:$KY(WO_4)_2$, exhibits a T_2 of 13.1 μs. Compared to other rare–earth–ion–doped crystals, like Pr^{3+}:Y_2SiO_5 that has a coherence time of more than 100 μs [8], or Eu^{3+}:Y_2SiO_5, which has a coherence time in the range of milliseconds [9], this value is rather short. It can be increased slightly by applying a magnetic field, but will remain in this order of magnitude. As there are crystals with much longer coherence times, it is unlikely that this crystal can advance the development of quantum gates.
Also, the value for the lifetime T_1, 44 μs, is rather short compared to the lifetimes of the other two mentioned crystals.

We expected the second crystal, Ho^{3+}:$LuVO_4$, to have a short coherence time, since we could not detect any photon echo. This assumption was confirmed as a result of the hole burning experiment, from which we obtained a value for T_2 in the nanosecond range. This very short coherence time eliminates the possibility of using this material for the construction of a quantum gate.
As the linewidth of the hole was very broad due to the short T_2, we could not get any information about hyperfine splitting in this crystal. The lifetime of the hole was measured to be 311 μs. Other crystals have hole lifetimes of days. So this lifetime is rather short, too. One possible explanation for the fact that both T_2 and the hole lifetime are quite short is the presence of strong magnetic interactions in this crystal.

Although we could not discover a material with adequate properties for the quantum computing project, it is nevertheless important to know about the inexpedience of these materials. The information obtained on these crystals was previously unknown and may be applied in other fields of research.

Acknowledgements

We are very grateful to Stefan Kröll for giving us the opportunity to carry out this project and for always helping us to approach the problems we met. We would like to thank our roommate Xuailiang Xu for his patience and the daily support in the lab.
Thanks also to Mattias Nilsson, Lars Rippe and Andreas Walther for their valuable advices and nice coffee breaks.
It was a great pleasure for us to be part of the photon echo group.

References

[1] Tomas Christiansson. *A first step towards Quantum Computing in Rare–earth–ion–doped crystals*, Master's thesis, Lund Reports on Atomic Physics LRAP–266, Lund Institute of Technology (2001)

[2] Nicklas Ohlsson. *Quantum Optics and Quantum Information Processing in Rare–Earth– Ion–Doped Crystals*, Doctoral thesis, Lund Reports on Atomic Physcis LRAP–300, Lund Institute of Technology (2003)

[3] Sven Andræ. *Stimulated Photon Echo & Photon Echo Relaxation Measurements*, Diploma paper, Lund Reports on Atomic Physics LRAP–124, Lund Institute of Technology (1991)

[4] M. Nilsson, L. Rippe, N. Ohlsson, T. Christiansson and S. Kröll. *Initial experiments concerning quantum information processing in rare–earth–ion–doped crystals*, Physica Scripta T102, 178 (2002)

[5] Sune Svanberg. *Atomic and Molecular Spectroscopy* (Springer Verlag, 2004)

[6] R.M. Macfarlane and R.M. Shelby. *Coherent Transient and Holeburning Spectroscopy of Rare Earth Ions in Solids* (North Holland, Amsterdam, 1987)

[7] Hans Hertz and Lars–Åke Nilsson. *Konstruktion och Testning av Digital Våglängdsmätare*, Lund Reports on Atomic Physics LRAP–1, Lund Institute of Technology (1980)

[8] R.W.Equall, R.L.Cone and R.M. Macfarlane. *Homogeneous broadening and hyperfine structure of optical transitions in* Pr^{3+}:Y_2SiO_5, Physical Review B, **52**, 3967 (1995).

[9] R.W. Equall, Y. Sun, R.L. Cone and R.M. Macfarlane. *Ultraslow Optical Dephasing in* Eu^{3+}:Y_2SiO_5, Physical Review **72**, 2180 (1994)

[10] Coherent Inc. *699 Ring dye laser instruction manual*

[11] V.S. Mironov, L.E. Li.*Crystal field analysis of* Pr^{3+} *and* Nd^{3+} *ions in* $KR(WO_4)_2$ *(R = Y or Gd) potassium rare–earth tungstates*, J. Alloys and compounds, **279**, 83 (1998)